ORIGINAL CONTRIBUTION

Removal of Pb^{2+} and Cd^{2+} by adsorption onto Y zeolite and its selectivity of retention in an actual contaminated effluent

Souhila Ait Hamoudi[1,2,3] · Nedjma Khelifa[2,3] · Loubna Nouri[1] · Sabra Hemidouche[1] · Amel Boudjemaa[1] ·
Youcef Boucheffa[2]

Abstract

The most important natural resource for human health and well-being is water, which can be affected by different sources, such as physical, organic, chemical, and microbiological ones. CBV 760 commercial zeolite was used and tested to remove inorganic pollutants, lead, and cadmium. Adsorption isotherms were used to assess the adsorption properties of contaminants and real effluent. At the solution pH (4.5 and 5), adsorption kinetics and isotherms were conducted for lead and cadmium, respectively. The investigated zeolite was quite efficient in lead and cadmium removal, as the maximal adsorbed amounts were $Q_a = 175$ and 148 mg g^{-1} for lead and cadmium, respectively, at $T = 308$ K. Adsorption capacity is pH dependent. Adsorption of Pb^{2+} and Cd^{2+} is highest at pH 8 ($Q_a = 107$ and 53.58 mg g^{-1}, respectively). The CBV 760 displays more affinity for Pb^{2+} than Cd^{2+}. It is worth noticing that CBV 760 exhibits good selectivity for heavy metal retention metals, namely, Ni^{2+}, Cu^{2+}, Cd^{2+}, and Pb^{2+}, in an actual contaminated effluent with a removal yield of 80% on CBV 760.

Keywords Adsorption · Water pollution · Heavy metals · Y zeolite · Porous materials · Water treatment

Introduction

Air and water pollution is a crucial problem in the modern world. Industrial chemicals, organic compounds, and fossil fuel use have attracted attention [1, 2]. The presence of metal ions (Ba^{2+}, Pb^{2+}, Cd^{2+}, Cr^{3+}, Cr^{6+}, Co^{2+}, Cu^{2+}, Ni^{2+}, Zn^{2+}, and Hg^{2+}) within the water is a problem that has caused environmental and health challenges in recent years [3].

Heavy metals exceed the density of 5 g/cm^3. Heavy metal reactivity and toxicity depend upon concentration and the ability of the heavy metal to be accumulated or transformed in living organisms. Environmental and toxicological properties depend on speciation. Heavy metal speciation is the state in which the molecule or ion appears in the environment.

The heavy metals are accumulated surreptitiously and reach the toxicity thresholds. Heavy metal releases identify the problems of heavy metal contamination in industrialized countries. As a result of cadmium and mercury contamination accidents [3–5]. Heavy metals occur in aquatic environments through both natural and anthropogenic sources. The exposure may result from direct releases into freshwater and marine ecosystems or through indirect streams such as dry and wet landfills and agricultural runoff. Some of the most relevant natural heavy metal sources are volcanic activity, contaminated continents, and wildfires. Volcanoes may contribute through either voluminous and sporadic volcanic activity-induced emissions or low-volume continuous emissions caused by magma outgassing and geothermal processes [6]. However, the main source of atmospheric mercury is the degassing of the earth's crust. Inconsiderate use and disposal of mercury in metallurgical and chemical industries lead to serious impacts; most of these heavy metals are ingested, stored, and even accumulated in the human body, which leads to chronic diseases [7–11]. Therefore, the rejected pollutants in the environment require attention to be removed from the wastewater. The processes of

✉ Souhila Ait Hamoudi
Souh_ait@yahoo.fr

1 Centre de Recherche scientifique et technique en Analyse Physico-Chimique (CRAPC), BP 384, Siège ex-Pasna Zone Industrielle, Bou-Ismail CP 42004, Tipaza, Algeria

2 Laboratoire LEPCMAE, Faculté de Chimie, Université des Sciences et de la Technologies Houari Boumediene (USTHB), B.P32 EL ALIA, Bab Ezzouar, Alger, Algeria

3 Ecole Nationale Supérieure des Sciences de la Mer et de lAménagement du Littoral, BP 19, Bois Des Cars, Dely Ibrahim, Alger, Algeria

adsorption, precipitation, solvent extraction, ion exchange, reverse osmosis, phytoremediation, flotation, filtration, sedimentation, electrochemical treatment, etc., are applied and further improved to treat heavy toxic metals from wastewater [12, 13]. The treatment of contaminated wastewater uses adsorption as a low-cost, environmentally friendly method. Heavy metal adsorption capacity study requires sludge [13], clays [14], silica gel, alumina, activated carbon [15], biochar and biochar-based composites [16], carbohydrate biopolymers [17], chitosan [18], and zeolites [19] as adsorbents. However, zeolites, which are inorganic crystalline polymers, may be used instead of activated carbon since the adsorption properties of such materials are significant. Zeolites are easily controlled (pore size variation, hydrophobicity, acidity, etc.) and are easily regenerated. Several fields use zeolites, such as adsorption, catalysis, and ion exchange. Among the various types of zeolites, the Y zeolite, which is considered a powerful molecular sieve with a Si/Al fraction of 1.5 to 3 and a skeleton geometry that is similar to that of the X zeolites and the uncommon mineral zeolite Faujasite, was identified by D. W. Breck to be the first successful exploration in this range of compounds [20]. The properties of the zeolite structure are the basis for its use in molecular adsorption. The ability to adsorb types of molecules rather than others confers a range of applications to zeolite as molecular sieves. Parameters that control access to the zeolite are the size and shape of pores; in other cases, several types of molecules penetrate the zeolite, and some diffuse through the channels fast, while the back of the zeolite retains other molecules, as in the paraxylene removal by Y zeolite [21]. Mintova records the particle size of Y zeolite [22] to be 60–70 nm and the channel size to be 7.4 Å. Herein is the removal of heavy metals (Pb^{2+} and Cd^{2+}) using a Y zeolite study. In the present work, the authors used a commercial zeolite labeled CBV 760 and tested it for the removal of inorganic pollutants, namely, lead and cadmium, and studied the sorption properties of CBV 760 through those pollutants and an actual effluent.

Materials and methods

All chemicals were analytical-grade reagents. For the preparation of aqueous solutions, use distilled water. Y zeolite (CBV 760) is a zeolyst brand. The NaOH and HCl were analytical Sigma-Aldrich products; the Pb $(NO_3)_2$ was from Riedel de Haën, of 99% purity; and the Cd $(NO3)_24H_2O$ was from Acrōs Organics, with a purity of 99%. Solutions of lead and cadmium were from Ficher Chemical commercial solutions at concentrations of 10,000 mg L^{-1} and 1000 mg L^{-1}, respectively. Successive dilutions of the stock solution are made until desired concentrations are obtained and analyzed by atomic absorption spectroscopy. The analysis

of atomic absorption spectroscopy was made with a varian AA240FS flame analyzer with an acetylene flame and a hollow cathode lamp as a light source ($\lambda = 217$ nm for lead and $\lambda = 228.8$ nm for cadmium). The SpectrAAv.5 software processes the results to obtain the residual concentrations of Pb^{2+} and Cd^{2+}.

Adsorption experiment

Adsorption kinetic

Adsorption kinetics of lead and cadmium were investigated in solutions with pH 4.7 and 5, respectively. In a controlled temperature bath (298 K), flasks were filled with 50 mL of a 100 mg L^{-1} solution of metal ions. Contact time ranged from 1 min to 24 h, with a stirring rate of 130 oscillations per minute. Then, the solution was centrifuged, and the supernatant was analyzed by atomic absorption spectroscopy (AAS). The empirical equations below were used to determine the adsorbed amount of metal ions onto the adsorbent and the Y (%) removal efficiency.

$$Q_t = \frac{V(C_0 - C_e)}{m} \tag{1}$$

$$Y(\%) = \frac{C_0 - C_e}{C_0} \times 100 \tag{2}$$

where C_0 and C_e are the initial and equilibrium metal ion concentrations in the solution (mg L^{-1}), V is the volume of the solution (L), and m is the adsorbent weight (g).

Effect of adsorbent dose

The operational conditions were the mass of the zeolite (60, 180, and 300 mg), contact times ranging from 1 min to 24 h, the pH of the medium, and the initial concentration of 100 mg L^{-1}, temperature of 298 K, and a stirring rate of 130 oscillations per minute were maintained.

Effect of metal ions initial concentration

The effect of pollutant initial concentration was investigated in this study. Therefore, the concentration was varied by 50, 100, and 150 mg L^{-1}.

Adsorption isotherm

Adsorption isotherms, which plot the adsorbed amount of pollutant against residual concentrations, were determined under the same experimental conditions as the adsorption kinetics by using a range of concentrations (25, 50, 100, 150, 200, 300, 400, 500, 600, 700, and 800 mg L^{-1}). Within

each solution (50 mL), the solution was kept in contact with 60 mg CBV 760 at 298 K for 24 h to ensure that equilibrium was reached.

Effect of temperature

The temperature effect was studied to determine the thermodynamic parameters. The adsorbed amounts of the selected pollutants were calculated at 308 and 318 K temperatures under the same experimental conditions (solution pH). The solution concentrations used for the present study were the same as those used for the adsorption isotherm study.

Effect of pH

The pH effect study uses 60 mg of zeolite to disperse in 50 mL of 150 mg L^{-1} solution to 298 K in 24 h. The solution pH is in the range of 2 to 8. To adjust the solutions, 0.1 N NaCl and NaOH solutions were used. Shake the suspensions for 24 h and centrifuge them. The equilibrium pH is measured using a pH meter (HANNA HI 123).

Sample characterization

The pH_{pzc} pH at the zero charge point of the CBV 760 zeolite was measured to understand its behavior toward metal ions. Therefore, a NaCl (0.1 N) solution was prepared and adjusted to the desired pH value in the range (2–12) with HCl and NaOH (0.1 N) solutions. The adjusted 50 mL solution was mixed with the sample for 24 h at 25 °C before being filtered to determine the equilibrium pH. A diffractometer D8 Advance (BRUKER-AXS) records the X-ray spectrum of CBV using copper radiation ($\lambda = 0.15418$ nm) at a scan range of $2\theta = 1–70°$ with a step size of 0.02°. FT-IR spectra were recorded in the wavenumber range 4000–400 cm^{-1} and acquired on an infrared Fourier transform (ALPHA, BRUKER spectrometer). An ASAP 2010 instrument measures the adsorption-desorption isotherms of N_2 at 77 K. To calculate the specific surface area, the Brunauer-Emmett-Teller (BET) method was used. [23]. The sample was characterized through a Quanta 250 scanning electron microscope (SEM) coupled to an energy-dispersive X-ray analyzer (EDX). An aluminum support coated with a self-adhesive graphite pellet powdered with sample.

The modeling adsorption kinetics

To investigate the Pb^{2+} and Cd^{2+} adsorption on CBV 760, pseudo-first order, pseudo-second order, and intra-particle diffusion rate equations were used to interpret experimental data. The pseudo-first-order Lagergren rate expression [24] as defined by the

$$\log\left(q_e - q_t\right) = \log q_e - \frac{k_1 t}{2.303} \tag{3}$$

Here, k_1 (g/ (min mg)) is the psedo-first-order model rate constant, and the plot of Ln ($q_e - q_t$) against t is used to determine k_1 and q_e values. The equation below expresses the pseudo-second-order rate equation of Ho [25]:

$$\frac{t}{q_t} = \frac{1}{k_2 q_e^2} + \frac{1}{q_e}t \tag{4}$$

The pseudo-second-order adsorption rate constant is k_2 (g mg^{-1} min^{-1}). The plot of t/q_t as a function of t is used to determine the k_2 and q_e values. In the intraparticle diffusion model, the relationship between q_t and $t^{0.5}$ [26] is written as

$$q_t = k_3 t^{0.5} + c \tag{5}$$

where k_3 (mg/g g min$^{0.5}$) is the rate of the intraparticle diffusion model and c is the line intercept proportional to the thickness of the boundary layer.

The modeling adsorption isotherms

Using the Freundlich isotherm model [27] to fit the experimental results of the Pb^{2+} and Cd^{2+} adsorption isotherms for all concentrations and the Langmuir model [28] by using Eqs. (6) and (7), respectively:

$$\log Q_a = \log K_F + \frac{1}{n}\log C_e \tag{6}$$

$$\frac{C_e}{Q_a} = \frac{1}{Q_m}C_e + \frac{1}{bQ_m} \tag{7}$$

where Q_a is the amount of pollutant adsorbed onto solids in milligrams per gram, and C_e (mg L^{-1}) is the residual concentration of Pb^{2+} and Cd^{2+}.

K_F and n were Freundlich constants related to the adsorption capacity and intensity, respectively, and K_L (L mg^{-1}) was a coefficient assigned to the affinity between the adsorbent and the adsorbate [29]. Another relevant parameter, R_L, commonly called the separation factor, is obtained from the relation (8) [30].

$$R_L = \frac{1}{1 + K_L C_0} \tag{8}$$

where C_0 is the concentration of the solute in the liquid phase. It was found that (i) $0 < R_L < 1$ indicates favorable adsorption, (ii) $R_L > 1$ indicates unfavorable adsorption, (iii) $R_L = 1$ indicates linear adsorption, and (iv) $R_L = 0$ indicates irreversible adsorption.

The usage of the normalized standard deviation to assess the agreement between measured and calculated values is expressed as follows:

$$\Delta q(\%) = \sqrt{\sum \frac{\left[\frac{(q_{exp} - q_{cal})}{q_{exp}}\right]^2}{n-1}} \times 100 \qquad (9)$$

Thermodynamic parameters

Free energy ($\Delta G°$) is used to determine the spontaneity of the system; this is obtained from the following equations [31]:

$$\Delta G° = -RT \ln K_d \qquad (10)$$

Thermodynamic parameters were calculated based on the below equation:

$$Ln\ K_d \frac{-\Delta H°}{RT} + \frac{\Delta S°}{R}$$
$$K_{d=\frac{q_e}{C_e}} \qquad (11)$$

Thermodynamic parameters are determined by the plot of ln $K_d = f(1/T)$, slope, and intercept are $-\frac{\Delta H°}{R}$ and $\frac{\Delta S°}{R}$, respectively.

Results and discussion

Characterization

Analysis infrared spectroscopy

Figure 1 shows the CBV 760 zeolite infrared spectrum.

The spectrum depicts bands at 529, 610, 680, 793, 837, 975, 1048, 1220, 1630, 1869, and 3430 cm^{-1}. The band at 975 cm^{-1} is due to the Si-O-Al anti-symmetric stretching vibrations in the T-O bonds (where T = Si or Al) [32–34].
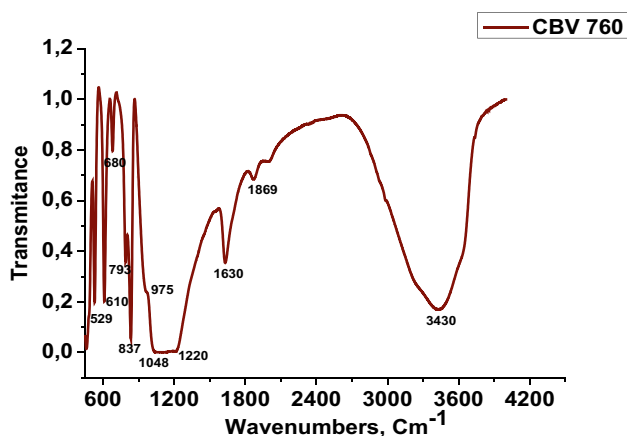
The 793 cm^{-1} band is due to the symmetric T-O-T elongation of S4R (single 4-ring) [35], while the 529 cm^{-1} absorption is attributed to the T-O-T symmetric stretching of the double 6-ring (D6R) [36]. Both bands at 610 and 680 cm^{-1} are assigned to the Si-O-Al symmetric elongation vibration and S4R symmetric bending modes [37], respectively. The 1048 cm^{-1} band is associated to asymmetric elongation modes of external links [38, 39], while bands at 837 and 1220 cm^{-1} are attributed to the symmetric and asymmetric elongation modes of the inner tetrahedra, respectively [40–43]. The 3430 cm^{-1} band corresponds to the bridged bond between Bronsted acid sites and OH groups and is found in the case of a protonated zeolite (CBV 760) [38, 44].

pH$_{pzc}$

Figure 2 represents the curve of pH at zero charge (pH$_{pzc}$). The pH$_{pzc}$ was determined to understand the surface chemistry of CBV 760. If the solution pH is lower than pH$_{pzc}$, the adsorbent surface is positively loaded, thus making the adsorption of metal ions (lead and cadmium) difficult [45]. Instead, the cationic adsorption occurs at a solution pH above pH$_{pzc}$.

Analysis by X-ray diffraction (XRD)

The X-ray diffraction (XRD) studies the high-crystallinity Y zeolite structure. Figure 3 displays the XRD pattern of CBV zeolite.

It was noticed that the sample spectrum in Fig. 3 showed a crystallinity identical to that of faujasite. The indicated peak positions are similar to those of Na-Y zeolite (the HY zeolite was synthesized from Na-Y zeolite), as reported in the COD card files (COD 96-900-0125).
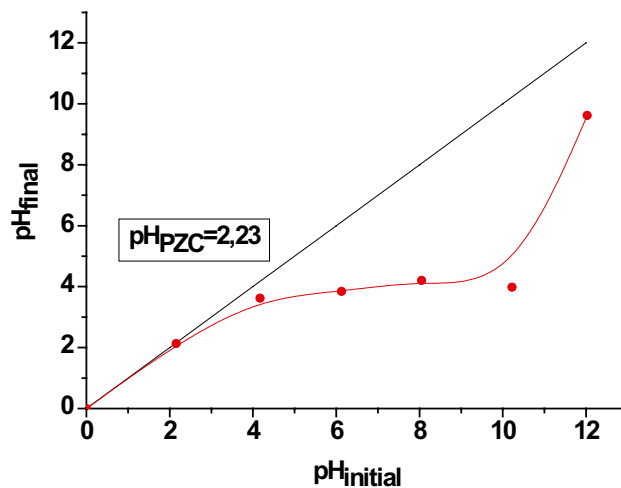

Fig. 1 The FTIR spectrum of CBV 760 zeolite

Fig. 2 pH dependence of adsorbent charge: determination of the Point of Zero Charge (PZC)
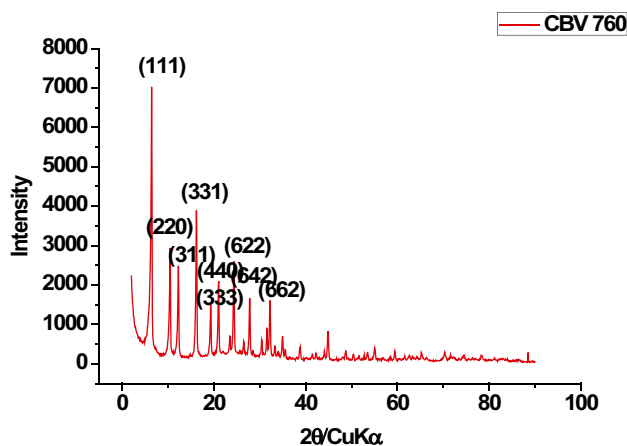
Fig. 3 XRD pattern of CBV zeolite

The sample belongs to the Faujasite-type Y zeolite class, and the zeolite is in the Fd 3 m cubic space group (cell parameter a = 24.24) [34, 46]. With a chemical formula of $H_{5.54}Na_{0.1}Al_{5.64}Si_{186.35}O_{384}$, it is HY (protonated shape).

N₂ adsorption–desorption

Figure 4 illustrates the adsorption–desorption isotherms of N_2 on CBV zeolite.

Based on the IUPAC classification, the isotherm shape is of type IV [47], with a hysteresis loop above $P/P_0 = 0.6$ of type H3, which indicates that the adsorption and desorption processes do not occur in the same way [48, 49], as a result of mesopore availability. In low pressure, the adsorption is sharp, demonstrating the presence of micropores. The plot of pore volume versus pore size of the sample allows to determine the pore distribution by the BJH method [50] in the relative pressure range $0 < P/P_0 < 0.35$, indicating that the pore distribution is focused between 10 and 15 Å (Fig. 4a), which corresponds to micropores ($D_p < 2$ nm). The pore distribution is shown in Fig. 4b and was for the pore diameter between 178 and 480 Å, which corresponds to mesopores ($2 < D_p < 50$ nm). To determine the microporous and mesoporous volumes, researchers employ the t-plot method. This involved plotting the volume of gas adsorbed (Vadsorbed) as a function of the thickness (t) of the adsorbate layer, resulting in the construction of a t-plot. By plotting the $V_{adsorbed}$ for CBV versus thickness (t), thus obtaining the t-plot. Surface area (S) was calculated based on BET theory using the following equation:

$$\frac{\frac{P}{P_0}}{V_{ads}(1 - \frac{P}{P_0})} = \frac{1}{V_{mono} \times C} + \frac{C - 1}{V_{mono} \times C} \times \frac{P}{P_0} \quad (12)$$
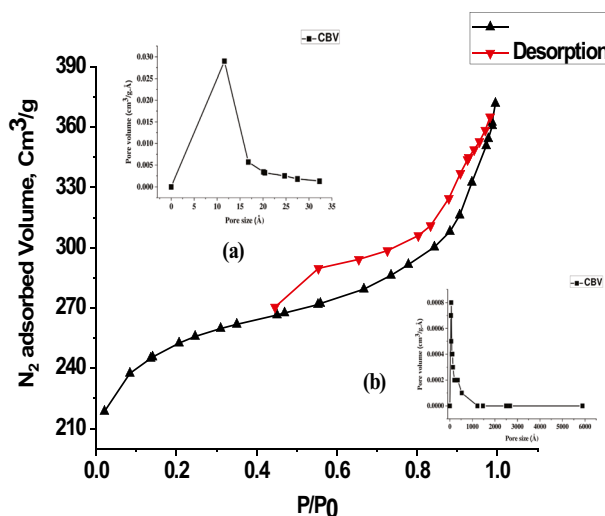

Fig. 4 The nitrogen adsorption/desorption isotherm of CBV 760

V_{ads} is the adsorbed volume of nitrogen in $Cm^3.g^{-1}$ at STP under pressure P.

V_{mono} is the volume of the monolayer of nitrogen adsorbed onto the solid in Cm^3g^{-1} at STP.

C is a constant that is characteristic of the interactions between adsorbate and adsorbent. V_{mono} and C are calculated by plotting $\frac{\frac{P}{P_0}}{V_{ads}\left(1 - \frac{P}{P_0}\right)}$ versus P/P_0 over a low-pressure range $0.05 < P/P_0 < 0.30$.

The S_{BET} specific surface ($m.^2$ / g) can therefore be calculated by the equation:

$$S_{BET} = \frac{V_{mono} \times N \times \sigma}{V_m} = 4,35 \times V_{mono} \quad (13)$$

V_m is the molar volume of a gas under normal temperature and pressure conditions (= 22415 Cm^3. $mole^{-1}$).σ is the cross-sectional area of the adsorbate at solid or liquid density, which is 16.2 Å for nitrogen.

N is the number of Avogadro = 6.023×10^{23} mol^{-1}.

The physicochemical characteristics of the studied CBV zeolite are summarized in Table 1.

Analysis by scanning electron microscopy (SEM)

The SEM method allows us to analyze the physical appearance, crystallinity, and crystal morphology of zeolite. The SEM result in Fig. 5a shows octahedral crystals, as expected from Y zeolite's high crystallinity. The EDX analysis (Fig. 5b) indicates that the Si/Al ratio of CBV zeolite is 4.53.
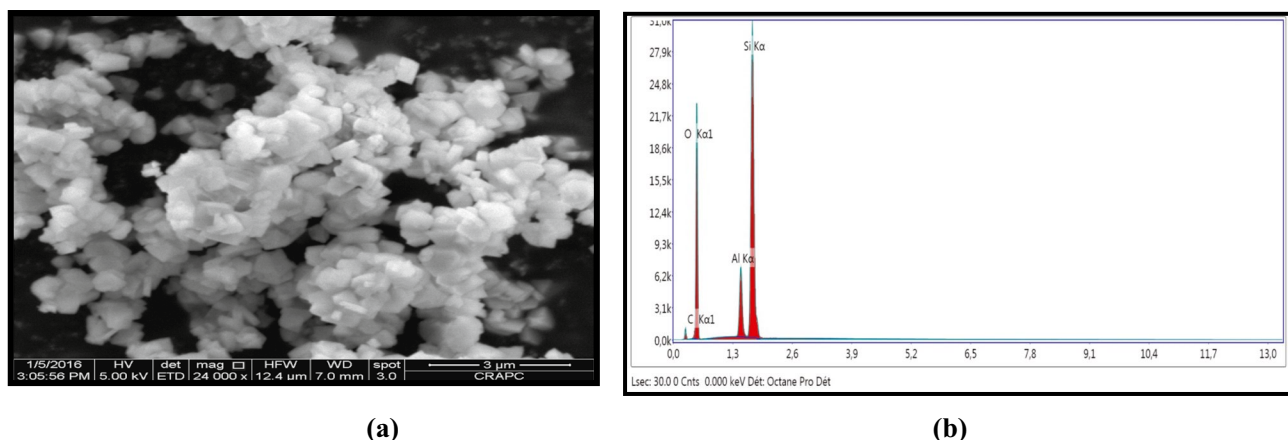
Table 1 Physico-chemical properties of CBV zeolite

S_{BET} (m²/g)	S_{ext} (m²/g)	S_{micro} (m²/g)	V_T (cm³/g)	V_{micro} (cm³/g)	V_{meso} (cm³/g)	Si/Al
739.42	258.78	480.64	0.575	0.275	0.363	4.53

(a)

(b)

Fig. 5 Scanning electron microscopy (**a**) and EDX analysis (**b**) of zeolite CBV760

Lead, cadmium adsorption

Adsorption kinetic

The Pb^{2+} and Cd^{2+} adsorption kinetics on CBV zeolite were studied over the contact time (Fig. 6) to determine the kinetic equilibrium time.

The adsorption kinetics reaches the equilibrium time within 30 min for lead and 15 min for cadmium. This difference in equilibrium time is due to the ionic radius of the two metals and their degree of electronegativity. The ionic radii are 0.98 and 0.78 A° for lead and cadmium, respectively. The metal with a small ionic radius (cadmium) diffuses before Pb^{2+} in the internal surface of the HY zeolite. In terms of electronegativity, the one with high electronegativity has an attraction for the single electrons of the functional groups (OH) on the surface of zeolite, as in the case of lead
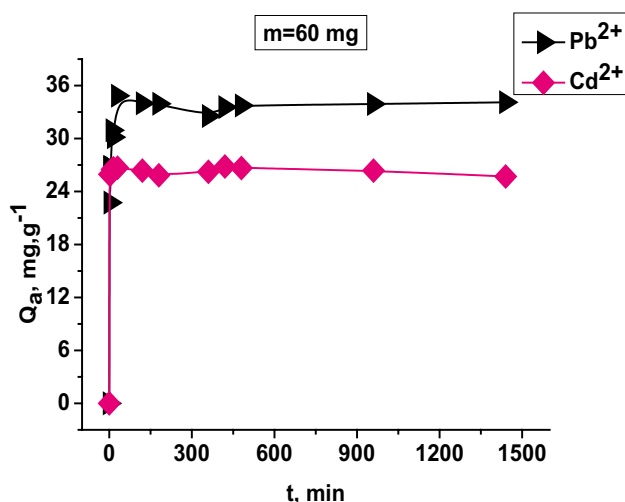
(2.33) compared to cadmium (1.69), hence a high adsorption capacity for Pb^{2+}.

The kinetic curve shows that the removal of metal ions was fast in the first few minutes due to surface adsorption. Curves are simple and lead to saturation because of the intra-particle diffusion process. Such a curve indicates the possibility of monolayer coverage of both metals on the CBV zeolite surface [51].

Effect of adsorbent dose

Pb^{2+} and Cd^{2+} adsorption kinetics onto the CBV 760 zeolite in a varied adsorbent dose range are displayed in Fig. 7.

Figure 7 shows that the adsorbed amount decreased with the increase in adsorbent mass; this is due to

(i)   The aggregation of particles and the increase in the diffusion path length led to a decrease in the total surface area of the adsorbent and a reduction in the adsorbed amount [52].

(ii) The high mass of adsorbent leads to saturated adsorption sites [53].

Effect of metal ions initial concentration

Figure 8 depicts how the adsorption capacity increases with increasing initial concentration.

Variations in the initial metal concentration may affect the adsorption efficiency through different factors, such as the availability of the surface functional groups and the ability of the surface functional groups to bond to the metal ion [54]. It was also the result of the driving force of the metal ions to the adsorption sites increasing as the initial concentration of the metal ions increased. Thus, the increase in the metal ion adsorbed amount per unit mass. Results shown in Fig. 8 indicate that the Pb^{2+} adsorbed amount is more than
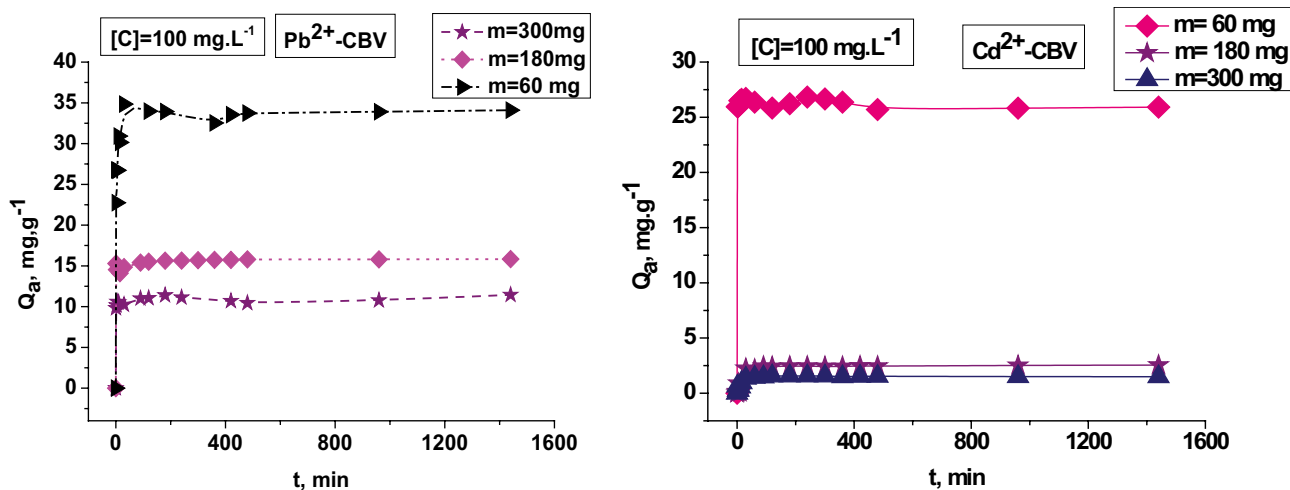

Fig. 6 Adsorption kinetics of Pb2+ and Cd2+ on CBV zeolite at 298 K, $m = 60$ mg, $[C] = 100$ mg.L^{-1}, pH 4.7 and 5 for Pb2+ and Cd2+, respectively

Fig. 7 The effect of adsorbent dose on retention capacity of Pb2+, Cd2+ on CBV at 298 K, $[C] = 100$ mg.L^{-1}, pH 4.7 and 5 for Pb2+ and Cd2+, respectively

that of Cd^{2+} due to the chemical and physical properties of the investigated metal ions, such as the atomic radius [55].

Effect of pH

The pH effect study assesses the retention behavior of heavy metals on the zeolite. The adsorbed amount (Q_a) of Pb^{2+} is higher than that of Cd^{2+} at the same pH value as intended (Fig. 9).

Regardless of the considered ion, the adsorbed amount (Q_a) is increased with pH and reaches a maximum in the pH range of 6–8. The increase in Q_a is relatively fast at pH values of 4–6. Indeed, the Pb^{2+} ion adsorption capacity increased as the pH increased from 4 to 6, from 24.83 to 106.66 mg. g^{-1}. For the Cd^{2+}, the adsorbed amount rises from 6.5 to 44.91 mg. g^{-1} with the increase in the Cd^{2+}

pH solution from 4 to 6. At high-acidic pH values, the H$^+$ ions are reported that compete with Pb^{2+} and Cd^{2+} ions for the adsorption sites upon the CBV zeolite. However, the electrostatic attraction of the dissolved ions to the surface charge controls the surface complexation reactions. Indeed, as cadmium and lead have ionic radii (0.97 and 1.20 Å), respectively, thus possess a low charge density and are hence more affected by surface group protonation [56] that reduces the adsorption sites on the CBV zeolite. As a result, fewer sites are available to uptake the studied metal ions. The metal ion adsorbed amount increases with the pH solution, reducing the competition of H$^+$ ions. For further explanation, surface hydroxyl sites can be yielded through functional group hydrolysis on the zeolite surface at alkaline pH values, which are beneficial for metal ion removal. Furthermore, the increase in the adsorbed amount of metal
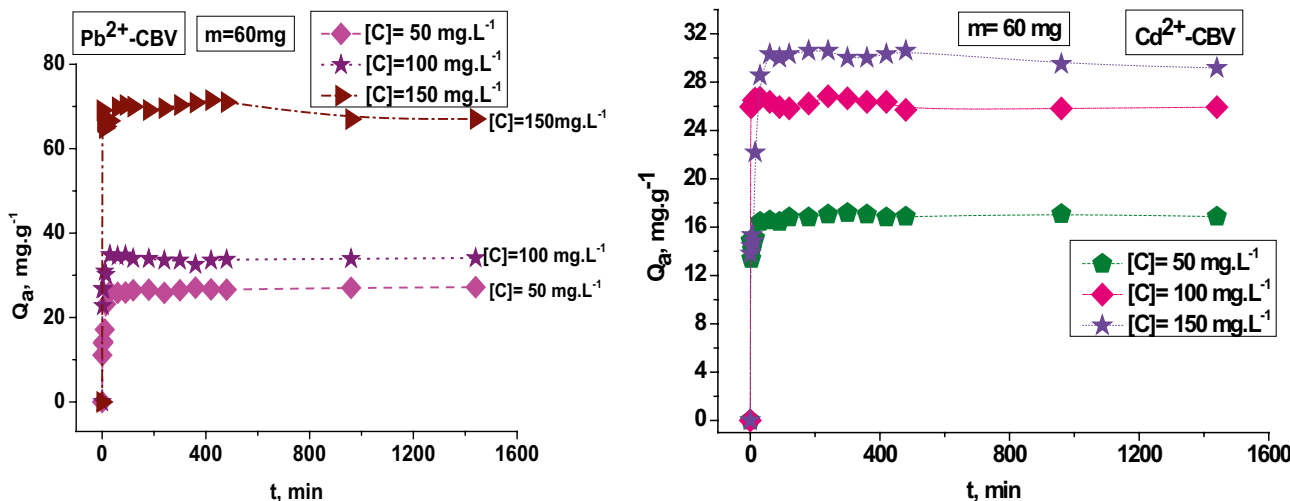

Fig. 8 Effect of metal ions initial concentration on retention of Pb2+, Cd2+ on CBV at 25 °C, $m = 60$ mg, pH 4.7 and 5 for Pb2+ and Cd2+, respectively
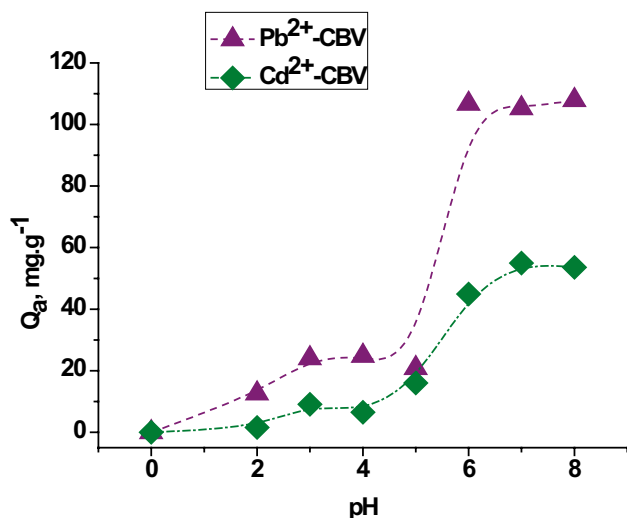
Fig. 9 pH Effect on adsorption of Pb2+ and Cd2+ onto CBV at 298 K, $m = 60$ mg, $[C] = 150$ mg.L^{-1}

ions is due to Pb^{2+} and Cd^{2+} ions hydration. Indeed, at pH > 8, Pb^{2+} and Cd^{2+} hydrate, forming the $PbOH^+$, $Pb(OH)$, and $Cd(OH)_2$ species [57] (precipitation of ions occurs within this pH range).

Adsorption isotherm

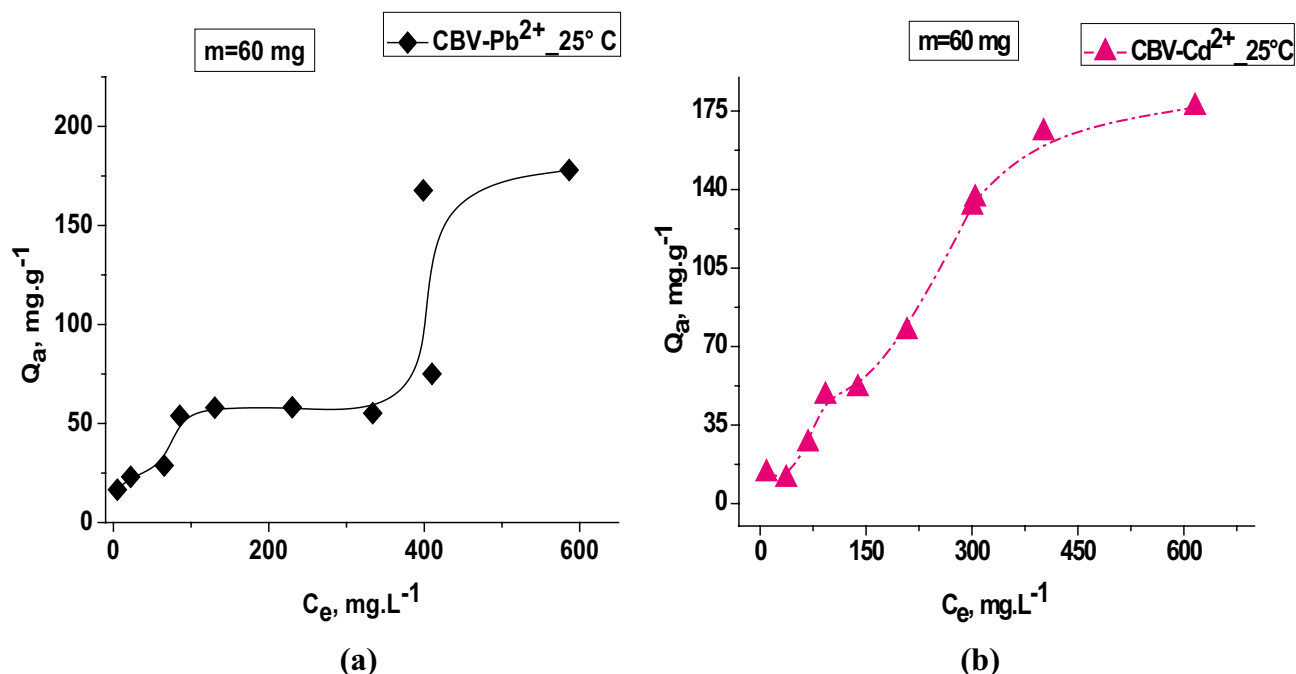Figure 10 depicts the adsorption isotherms of Pb^{2+} and Cd^{2+} on CBV zeolite.

The maximum CBV adsorption amounts are 178 and 176 mg. g^{-1}, with residual concentrations of 586.45 mg. L^{-1} and 616 mg. L^{-1}, for lead and cadmium, respectively, as shown in Fig. 10. The Pb^{2+} and Cd^{2+} adsorption isotherms onto CBV zeolite are of S type by the classification of Giles [58]. Such isotherms indicate an intense competition for the adsorption sites between the solvent molecules and the studied ions. S-shaped curves characterize the wide pore sizes of the adsorbents. This kind of curve with an inflection point in Fig. 10a is associated with the successive adsorption process that occurs in the case of metal cation adsorption through the functional groups on the adsorbent surface with various mechanisms of interactions between the adsorbate and the functional groups, as reported by Neskoromnaya et al. [59]. Adsorption of lead and cadmium on zeolite occurs in two steps: the first one is a monolayer (Langmuir) in the low concentration range, and the second one is a multilayer (Freundlich) in the high concentration range. As the solution concentration increases, the adsorption becomes easier, reaching saturation when adsorbed ions occupy all adsorbent receptor sites. Thus, a single layer of adsorbate (a monolayer) forms.

Effect of temperature on adsorption of Pb^{2+} and Cd^{2+} onto CBV zeolite

Temperature is a relevant thermodynamic parameter that can impact the adsorption on a solid surface. Indeed, adsorption
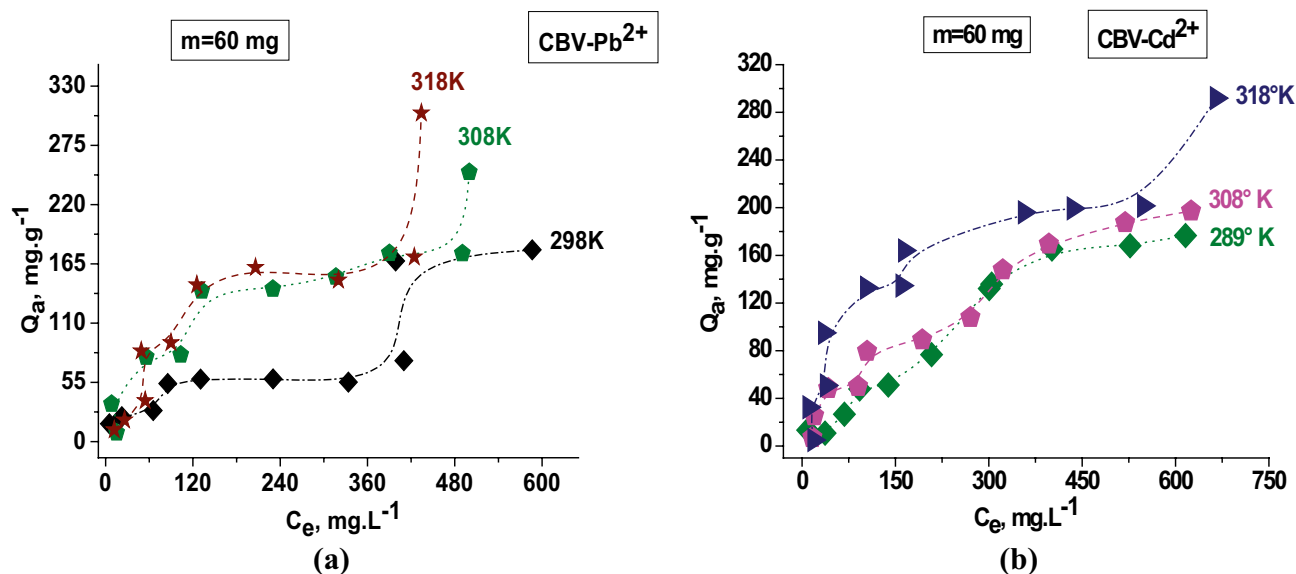

Fig. 10 Adsorption isotherm of Pb2+ (**a**) and Cd2+ (**b**) on CBV zeolite at 298 K, pH 4.5 and 5 (the solution pH of Pb2+ and Cd2+, respectively)

Fig. 11 Temperature effect on adsorption of Pb2+(**a**) and Cd2+(**b**) onto CBV zeolite, $m=60$ mg, pH 4.7 and 5 for Pb2+ and Cd2+, respectively

is a physical process related to the molecular interactions between a liquid or gas phase and the adsorbent surface. The temperature effect may modify these interactions [60, 61].

The result in Fig. 11 demonstrates that for all investigated temperatures (298, 308, and 318 K), the Pb^{2+} adsorbed amount (Q_a) on the CBV is more than that for Cd^{2+}. Indeed, considering the temperature of 308 K and at the same initial concentration (C_0) of Pb^{2+} and Cd^{2+} of 500 mg. L^{-1} Q_a is 175 mg. g^{-1} and 148 mg. g^{-1}. These adsorbed amounts correspond to the respective residual concentrations (C_e) of 316 and 322 mg. L^{-1}. However, the driving force of metal ions to the active sites of the CBV zeolite may accelerate with the increase in temperature [62, 63].

The modeling adsorption kinetics of Pb^{2+} and Cd^{2+} onto CBV

The results (the rate constants and R^2 correlation coefficients) in Tables 2 and 3 are from modeling the adsorption kinetics of Pb^{2+} and Cd^{2+} using the pseudo-first-order (PFO), pseudo-second-order (PSO), and intraparticle models.

The pseudo-second-order model (PSO) fits the experimental adsorption kinetics of Pb^{2+} and Cd^{2+}. The R^2 values are close to one, and the PSO q_e values proximate to the

experimental data support the obtained result. A comparison of the standard deviations of the two models finds that Δq (%) is low for the PSO model compared to the PFO model. This statement is for both studied metal ions. The q_e value determined by the PSO model is 68.49 mg. g^{-1}, close to the experimental value of 69.80 mg. g^{-1}. Concerning the cadmium, the value of q_e calculated by the PSO model is 30.47 mg. g^{-1}, close to the experimental value, which is 30.30 mg. g^{-1}, in contrast to the PFO model. (Table 2). That result suggests that Pb^{2+} and Cd^{2+} adsorption might be a chemisorption [64]. The modeling of the adsorption kinetics uses the intraparticle model to further understand the adsorption by plotting q_t versus $t^{0.5}$. If the pattern is linear and passes through the origin, the adsorption follows the intraparticle diffusion model. However, if an external mass transfer or chemical reaction is involved, the straight line does not pass through the origin [65, 66].

The multilinearity obtained in the graph (figure not shown) implies that two or more reactions occur [67, 68]. The rate constants express the different stages of adsorption, and the variation of these constants can be due to the surface adsorption stages (Fig. 12). Heavy metals (Pb^{2+}, Cd^{2+}) are adsorbed fast by the outer adsorbent surface. Nevertheless, after the external surface is saturated, the heavy metals

Table 2 Kinetic model parameters attributed to lead and cadmium

Models	Pseudo-first order (PFO) (Lagergren)				Pseudo-second order (PSO)			
	q_e (mg.g^{-1})	K_1 (min^{-1})	R^2	Δq (%)	q_e (mg.g^{-1})	K_2 (g.mg. min^{-1})	R^2	Δq (%)
Pb^{2+}	7.38	0.014	0.6207	40.01	68.49	0.0026	0.9994	31.36
Cd^{2+}	20.49	0.07	0.6527	23.12	30.47	0.0079	0.9996	18.30

Table 3 Determination of intraparticular model rate constants to lead and cadmium onto CBV

Ions	Pb^{2+}					Cd^{2+}					
Parameters	Step 1	Step 2	Step 3	Step 4	Step 5	Step 1	Step 2	Step 3	Step 4	Step 5	Step 6
R^2	-	−0.333	−0.750	0.8660	-	-	0.6721	−0.82	0.8042	0.7945	-
K_{dintr} (mg/g min^{0,5})	69.10	0.0627	0.0134	0.0106	0.006	13.804	2.0127	0.1886	0.130	0.0963	−0.048

penetrate the adsorbent particles and adsorb onto the inner surface of the adsorbent. Therefore, the heavy metals diffuse into the adsorbent pores. This stage represents the final stage and reaches equilibrium, indicating that the intraparticle diffusion becomes slow due to the low solute concentrations in the solution and thus leads to a decrease in the rate constants [69, 70] (Table 3).

Adsorption mechanism of metal ions (Pb^{2+} and Cd^{2+}) onto CBV zeolite

This study showed that heavy metals diffuse into the adsorbent pores, which indicates slow diffusion of ions into the internal channels of the zeolite. Then, the ions move to the position of exchangeable ions within the crystal structure [71–73]. Ion exchange occurs between the exchangeable cations (Ca^{2+}, Na$^+$, and K$^+$) in the crystal structure of the zeolite and the metal ions (Pb^{2+} and Cd^{2+}). The HY zeolite is porous, characterized by SiO$_4^{4-}$ and AlO$_4^{5-}$ tetrahedra linked by their oxygen. The coexistence of aluminol and silanol groups leads to a Bronsted and Lewis acidity. The adsorption of metal ions takes place at the pH of the solution (pH 4.5 for cadmium and pH 5 for lead) without

adjustment. Within the acidic medium, the oxygen of aluminol and silanol groups releases a proton and forms a negative charge. The functional groups that contain oxygen are mainly involved in metal ion adsorption. By electrostatic attraction, the negative charge attracts the adsorbed metal ions to create a complex on the inner sphere adsorbent surface. That leads to the formation of the Pb-(Cd)-O bond, and the covalent bonds Pb-O-Si and Cd-O-Si promote the adsorption due to the presence of high adsorbent-adsorbate interactions [74]. Thus, the ion exchange, electrostatic, and surface complexes mechanisms govern the adsorption process [74, 75].

Modeling adsorption isotherms

The modeling of adsorption isotherms uses the Freundlich and Langmuir models for the studied temperatures (298, 308, and 318 K). Table 4 shows the obtained results.

Table 4 shows that the K_L parameter (which gives information about the adsorbate-adsorbent bond) of the Langmuir model and the adsorbed amount (Q_m) increase with the increase in temperature. Therefore, the bond between metallic ions and the CBV strengthens as the temperature rises. The K_L constant of Pb^{2+} is greater than that of Cd^{2+}
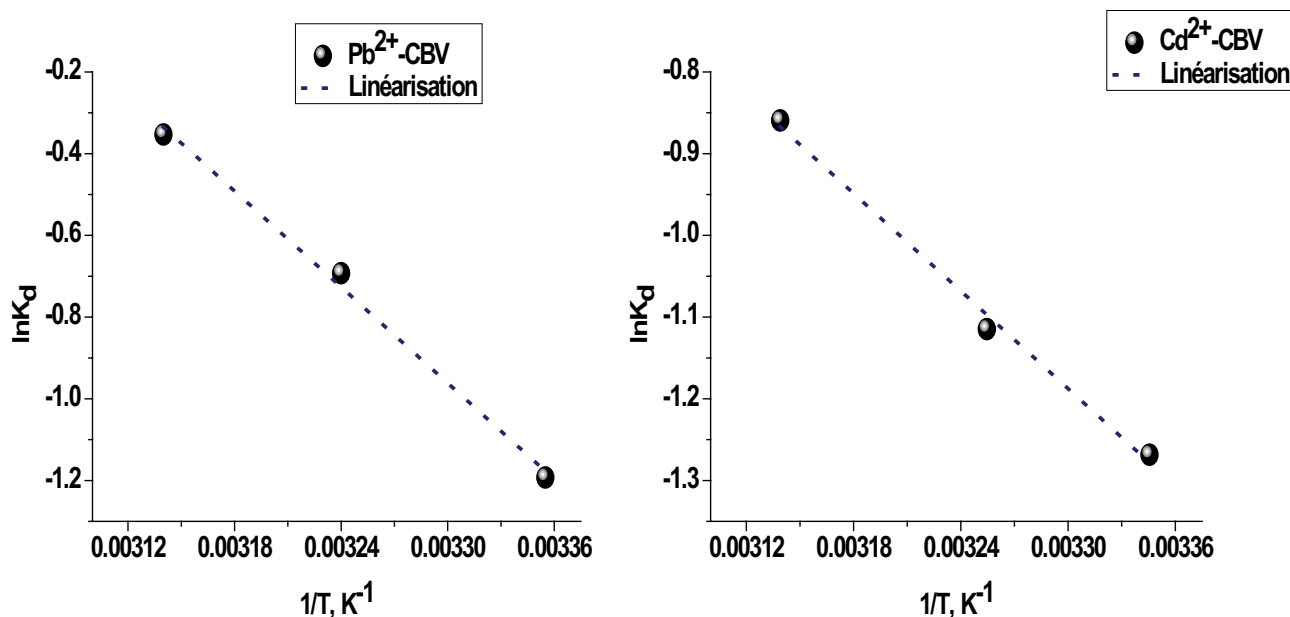

Fig. 12 Variation of Pb2 + and Cd2 + adsorption constant onto CBV as a function of temperature

Table 4 Model parameters Langmuir and Freundlich of adsorption of metal ions (Pb^{2+}, Cd^{2+}) onto CBV at different temperatures

Metal ions	Temperature (K)	Langmuir					Freundlich			
		Q_m (mg.g^{-1})	K_L (L.mg^{-1})	R_L	R^2	Δq (%)	K_F (L.mg^{-1})	$1/n$	R^2	Δq (%)
Pb^{2+}	298	57.47	0.172	0.666–0.058	0.9965	36.8	2.43×10^{-4}	2.11	0.9745	43.8
	308	244.5	2.04	0.019–0.000610	0.9999	26.54	1.68	0.80	0.8411	50.91
	318	303.030	3.30	0.012–0.000378	0.9992	38.74	1.56	0.83	0.9104	45.26
Cd^{2+}	298	175.43	0.023	0.631–0.0515	0.9647	34.04	14.41	0.98	0.9529	44.34
	308	192.30	0.060	0.398–0.0204	0.9954	30.60	4.51	0.56	0.9579	40.97
	318	290.70	0.063	0.388–0.0194	0.9641	36.45	0.90	0.45	0.9135	53.85

for the investigated isotherms. Hence, the CBV-Pb^{2+} bond is high than that of CBV-Cd^{2+}. The Q_m values obtained by the Langmuir model are close to experimental values at the same temperature. Indeed, at $T = 318$ K, $Q_m = 303.03$ mg. g^{-1} for Pb^{2+}, which is close to that obtained by the experiment of 304 mg. g^{-1}. The $Q_m = 290.70$ mg. g^{-1} (from the Langmuir model) for Cd^{2+} is close to 291 mg. g^{-1} (from the experiment). However, the R_L parameter is in the $0 < R_L < 1$ range, which indicates that the Langmuir isotherm is favorable, and the standard deviations Δq (%) are less than those of the Freundlich model. Therefore, the metal ion adsorption is monolayer, which means the surface is homogeneous. The interactions between the adjacent adsorbed ions are non-lateral when a single ion occupies a single surface site [76]. Except for the Cd^{2+} adsorption isotherm over CBV at $T = 318$ K, the Freundlich model is almost not fitted to the obtained results due to the R^2 correlation coefficient, which is $R^2 < 1$ despite $n > 1$ (favorable isotherm) [77, 78]. The Freundlich model can be used for non-homogeneous surfaces and considers that the concentration of the adsorbed ionic species on the solid surface increases as the concentration of certain species in the liquid phase is enhanced [79, 80].

Thermodynamic study

The thermodynamic of the adsorption requires the knowledge of two thermodynamic parameters: the free enthalpy ($\Delta G°$) and the entropy ($\Delta S°$) [81, 82].

The thermodynamic parameters $\Delta H°$ (kJ. mol^{-1}), $\Delta S°$ (kJ K^{-1}. mol^{-1}), Δ and $G°$ (kJ. mol^{-1}) of Pb^{2+} and Cd^{2+} adsorption on CBV at different temperatures are in Table 5.

The $\Delta H°$ value is lower than 40 kJ. mol^{-1} (which indicates the interaction energy between adsorbate-adsorbent) and positive for Pb^{2+} and Cd^{2+} adsorption on CBV. It reveals a strong bond between the metallic ions and the CBV zeolite and proves that the Pb^{2+} and Cd^{2+} ions adsorption process is endothermic. [83, 84]. Adsorption metal ion kinetic modeling suggested that the adsorption may be a chemisorption. The thermodynamic study determined that the adsorption process is physical adsorption since the free enthalpy < 40 kJ. mol^{-1} [85].

During the adsorption of metal ions, structural changes at the adsorbate-adsorbent lead to a positive entropy. That increases the disorder during the adsorption of Pb^{2+} and Cd^{2+} on the CBV 760 zeolite [86, 87]. The result in Table 5 shows that the standard free enthalpy $\Delta G°$ decreases with the increase in temperature, indicating a spontaneous adsorption onto CBV zeolite [88, 89].

Adsorption of an actual contaminated battery effluent on CBV zeolite

The adsorption study of lead and cadmium from a synthetic solution onto CBV zeolite is efficient. The aim is to investigate the performance of CBV zeolite through heavy metals in an actual contaminated effluent, which is an R_0 effluent issued from the battery manufacturing company from Oued S'mar (Algiers, Algeria). The experimental conditions are the same as those of the Pb^{2+} and Cd^{2+} adsorption kinetics. Table 6 displays the various concentrations of metal ions in R_0 before CBV contact.

Table 5 Thermodynamic parameters of Pb^{2+} and Cd^{2+} adsorption onto CBV

Metal ions	Temperature (Kelvin)	$\Delta H°$ (kJ.mol^{-1})	$\Delta S°$ (kJK^{-1}.mol^{-1})	$\Delta G°$ (kJ.mol^{-1})
Pb^{2+}	298	32.58	0.09950	2.93
	308			1.93
	318			0.94
Cd^{2+}	298	16.56	0.04476	3.22
	308			2.77
	318			2.32

Table 6 Concentration of R_0, R_1 before and after contact with CBV

Samples	Metals	Concentration (mg.L^{-1})	Q_a (mg.g^{-1})	Y (%)
R_0	Pb^{2+}	78.9	-	-
	Cd^{2+}	6.52	-	-
	Cu^{2+}	0.54	-	-
	Ni^{2+}	0.26	-	-
R_1	Pb^{2+}	21.9	47.5	72.24
	Cd^{2+}	1.26	4.38	80.67
	Cu^{2+}	0.15	0.32	72.22
	Ni^{2+}	0.12	0.11	53.84

After the CBV zeolite contact, the supernatant is recovered after centrifugation and analyzed by AAS. Table 6 shows the results.

Table 6 displays that the removal capacity of heavy metals onto CBV follows the order: $Ni^{2+} < Cu^{2+} < Cd^{2+} < Pb^{2+}$ in R_1. Due to the selectivity of CBV for lead and cadmium and their ion exchange capacities during the adsorption, the adsorbent exhibited high removal efficiency for these heavy metals. [90–92]. Results reported in Table 6 indicate a high capacity of the CBV for heavy metal removal from an actual contaminated battery effluent.

Conclusion

The present study uses a commercial faujasite Y zeolite (CBV 760) to remove heavy metal (Pb^{2+} and Cd^{2+}) from synthetic solution and actual contaminated battery effluent. The adsorption efficiency of CBV 760 zeolite towards heavy metals such as Pb^{2+} and Cd^{2+} was tested. The adsorption kinetic of Pb^{2+} is fast compared to that of Cd^{2+}. The adsorption kinetics reveals that the adsorption of Pb^{2+} and Cd^{2+} depends on the contact time, the adsorbent mass, the pH of the solution, the initial concentration, and the temperature. The comparative study of adsorption isotherms of (Pb^{2+}, Cd^{2+}) on Y zeolite (CBV 760) shows that the lead was better adsorbed than cadmium in synthetic solution and real contaminated effluent due to the physicochemical properties of both pollutants. Therefore, the CBV 760 can be used to deal with environmental problems due to the cages and supercages that characterize the zeolite, which confer it the highly porous texture, and also due to the high specific surface area, which provides the capacity to remove pollutants.

Declarations

Competing interests The authors declare no competing interests.

References

1. Li Y, Wang J-D, Wang X-J, Wang J-F (2012) Adsorption–desorption of Cd(II) and Pb(II) on Ca-Montmorillonite. nd Eng Chem Res 51(18):6520–6528. https://doi.org/10.1021/ie203063s
2. Gong J, Liu T, Wang X, Hu X, Zhang L (2011) Efficient Removal of heavy metal ions from aqueous systems with the assembly of anisotropic layered double hydroxide nanocrystals@carbon nanosphere. Environ Sci Technol 45(14):6181–6187. https://doi.org/10.1021/es200668q
3. Goldberg ED (1979) La santé des océans. Unesco, Paris, p 188
4. Nitta T (1972) MpiJ. Marine Pollution and Sea Life, edby M. Surrey, Fishing News (Books), Ruivo. West Byfleet, pp 77–81
5. Kurland LT (1960) SNF, H. SIEDLER Minamata disease. The outbreak of a neurologic disorder in Minamata, Japan, and its relationship to the ingestion of seafood contaminated by mercuric compounds. World Neurol 1:370–395
6. Agarwal SK (2009) HMP, Published by SB. Nangia A P H Publishing Corporation 4435–36/7:227
7. Simeonidis K, Mourdikoudis S, Kaprara E, Mitrakas M, Polavarapu L (2016) Inorganic engineered nanoparticles in drinking water treatment: a critical review. Environ Sci Water Res Technol 2(1):43–70. https://doi.org/10.1039/C1035EW00152H
8. Turhanen PA, Vepsäläinen JJ, Peräniemi S (2015) Advanced material and approach for metal ions removal from aqueous solutions. Sci Rep 5(1):8992. https://doi.org/10.1038/srep08992.10.1038/srep08992
9. Ciszewski D, Grygar TM (2016) A review of flood-related storage and remobilization of heavy metal pollutants in river systems. Water Air Soil Pollut 227(7):239. https://doi.org/10.1007/s11270-11016-12934-11278
10. Fu F, Wang Q (2011) Removal of heavy metal ions from wastewaters: a review. J Environ Manage 92(3):407–418. https://doi.org/10.1016/j.jenvman.2010.1011.1011
11. Razak NHA, Praveena SM, Aris AZ, Hashim Z (2015) Drinking water studies: a review on heavy metal, application of biomarker and health risk assessment (a special focus in Malaysia). J Epidemiol Glob Health 5(4):297–310. https://doi.org/10.1016/j.jegh.2015.1004.1003
12. Shanker AK (2019) Chromium: environmental pollution, health effects and mode of action☆. In: Nriagu J (ed) Encyclopedia of Environmental Health (Second Edition). Elsevier, Oxford 624–633. https://doi.org/10.1016/B1978-1010-1012-409548-409549.411575-409541
13. Mohy Eldin MS, Abu-Saied MA, Tamer TM, Youssef ME, Hashem AI, Sabet MM (2016) Development of polystyrene based nanoparticles ions exchange resin for water purification applications. Desalin Water Treat 57(32):14810–14823. https://doi.org/10.11080/19443994.19442015.11080192
14. Zhu R, Chen Q, Zhou Q, Xi Y, Zhu J, He H (2016) Adsorbents based on montmorillonite for contaminant removal from water: a review. Appl Clay Sci 123:239–258. https://doi.org/10.1016/j.clay.2015.1012.1024
15. Jurado-Sánchez B, Sattayasamitsathit S, Gao W, Santos L, Fedorak Y, Singh VV, Orozco J, Galarnyk M, Wang J (2015) Self-propelled activated carbon janus micromotors for efficient water purification. Small 11(4):499–506. https://doi.org/10.1002/smll.201402215
16. Liang L, Xi F, Tan W, Meng X, Hu B, Wang X (2021) Review of organic and inorganic pollutants removal by biochar and biochar-based composites. Biochar 3(3):255–281. https://doi.org/10.1007/s42773-42021-00101-42776

17. Fouda-Mbanga BG, Prabakaran E, Pillay K (2021) Carbohydrate biopolymers, lignin based adsorbents for removal of heavy metals (Cd2+, Pb2+, Zn2+) from wastewater, regeneration and reuse for spent adsorbents including latent fingerprint detection: a review. Biotechnol Rep 30:e00609. https://doi.org/10.01016/j.btre.02021.e00609

18. Renu AM, Singh K (2016) Heavy metal removal from wastewater using various adsorbents: a review. J Water Reuse Desalin 7(4):387–419. https://doi.org/10.2166/wrd.2016.2104

19. Ghasemi Z, Sourinejad I, Kazemian H, Rohani S (2018) Application of zeolites in aquaculture industry: a review. Rev Aquac 10(1):75–95. https://doi.org/10.1111/raq.12148

20. Flanigen EM (1984) Molecular sieve zeolite technology: the first twenty-five years. In: Ribeiro FR, Rodrigues AE, Rollmann LD, Naccache C (eds) Zeolites: Science and Technology. Springer Netherlands, Dordrecht 3–34. https://doi.org/10.1007/1978-1094-1009-6128-1009_1001

21. de Magalhães LF, da Silva GR, Peres AEC (2022) Zeolite application in wastewater treatment. Adsorpt Sci Technol 2022:4544104. https://doi.org/10.1155/2022/4544104

22. Mintova S (2003) Nanosized molecular sieves. Collect Czech Chem Commun 68:2032–2054. https://doi.org/10.1135/cccc20032032

23. Brunauer S, Emmett PH, Teller E (1938) Adsorption of gases in multimolecular layers. J Am Chem Soc 60(2):309–319. https://doi.org/10.1021/ja01269a01023

24. Yuh-Shan H (2004) Citation review of Lagergren kinetic rate equation on adsorption reactions. Scientometrics 59(1):171–177. https://doi.org/10.1023/B:SCIE.0000013305.0000099473.cf

25. Ho YS, McKay G (1998) Sorption of dye from aqueous solution by peat. Chem Eng J 70(2):115–124. https://doi.org/10.1016/S0923-0467(1098)00076-00071

26. Guibal E, Milot C, Tobin JM (1998) Metal-anion sorption by chitosan beads: equilibrium and kinetic studies. Ind Eng Chem Res 37(4):1454–1463. https://doi.org/10.1021/ie9703954

27. Freundlich H (1907) Über die Adsorption in Lösungen. Z Phys Chem 57U(1):385–470. https://doi.org/10.1515/zpch-1907-5723

28. Langmuir I (1918) The adsorption of gases on plane surfaces oF glass, mica and platinum. J Am Chem Soc 40(9):1361–1403. https://doi.org/10.1021/ja02242a02004

29. Oubagaranadin JUK, Murthy ZVP (2010) Isotherm modeling and batch adsorber design for the adsorption of Cu(II) on a clay containing montmorillonite. Appl Clay Sci 50(3):409–413. https://doi.org/10.1016/j.clay.2010.1009.1008

30. McKay G, Bino MJ, Altamemi AR (1985) The adsorption of various pollutants from aqueous solutions on to activated carbon. Water Res 19(4):491–495. https://doi.org/10.1016/0043-1354(1085)90041-90047

31. Namasivayam C, Senthilkumar S (1997) Recycling of industrial solid waste for the removal of mercury (II) by adsorption process. Chemosphere 34(2):357–375. https://doi.org/10.1016/S0045-6535(1096)00383-00389

32. Mozgawa W (2001) The relation between structure and vibrational spectra of natural zeolites. J Mol Struct 596(1):129–137. https://doi.org/10.1016/S0022-2860(1001)00741-00744

33. Joshi UD, Joshi PN, Tamhankar SS, Joshi VV, Rode CV, Shiralkar VP (2003) Effect of nonframework cations and crystallinity on the basicity of NaX zeolites. Appl Catal A: Gen 239(1):209–220. https://doi.org/10.1016/S0926-1860X(1002)00391-00395

34. Dabbawala AA, Vaithilingam BV, Mittal H, Wahedi YA, Khan S, Joseph T, Singaravel G, Morin S, Berthod M, Alhassan SM (2020) Synthesis and catalytic performance of zeolite-Y supported on silicon carbide in n-heptane cracking. Appl Catal A: Gen. https://doi.org/10.1016/j.apcata.2020.117866

35. Hamidi R, Khoshbin R, Karimzadeh R (2021) A new approach for synthesis of well-crystallized Y zeolite from bentonite and rice husk ash used in Ni-Mo/Al2O3-Y hybrid nanocatalyst for hydrocracking of heavy oil. Adv Powder Technol 32(2):524–534. https://doi.org/10.1016/j.apt.2020.1012.1029

36. Zhang R, Xu S, Raja D, Khusni NB, Liu J, Zhang J, Abdulridha S, Xiang H, Jiang S, Guan Y, Jiao Y, Fan X (2019) On the effect of mesoporosity of FAU Y zeolites in the liquid-phase catalysis. Micropor Mesopor Mat 278:297–306. https://doi.org/10.1016/j.micromeso.2018.1012.1003

37. Tolentino CMC, de Luna MDG, Futalan CM, Choi AES, Manegdeg FG, Grisdanurak N (2020) Influence of hydrocarbons on hydrogen chloride removal from refinery off-gas by zeolite NaY derived from rice husks. Sci Total Environ. https://doi.org/10.1016/j.scitotenv.2020.138782

38. Karge HG (1998) Characterization by infrared spectroscopy. Micropor Mesopor Mat 22(4):547–549. https://doi.org/10.1016/S1387-1811(1098)80021-80028

39. Oruji S, Khoshbin R, Karimzadeh R (2018) Preparation of hierarchical structure of Y zeolite with ultrasonic-assisted alkaline treatment method used in catalytic cracking of middle distillate cut: the effect of irradiation time. Fuel Process Technol 176:283–295. https://doi.org/10.1016/j.fuproc.2018.1003.1035

40. McCusker LB, Baerlocher C (2001) Chapter 3 Zeolite structures. In: van Bekkum H, Flanigen EM, Jacobs PA, Jansen JC (eds) Studies in surface science and catalysis, vol 137. Elsevier 37–67. https://doi.org/10.1016/S0167-2991(1001)80244-80245

41. Jentys A, Lercher JA (2001) Chapter 8 Techniques of zeolite characterization. In: van Bekkum H, Flanigen EM, Jacobs PA, Jansen JC (eds) Studies in Surface Science and Catalysis, vol 137. Elsevier 345–386. https://doi.org/10.1016/S0167-2991(1001)80250-80250

42. Hassan H, Hameed BH (2011) Oxidative decolorization of acid red 1 solutions by Fe–zeolite Y type catalyst. Desalination 276(1):45–52. https://doi.org/10.1016/j.desal.2011.1003.1018

43. Zhu L, Lv X, Tong S, Zhang T, Song Y, Wang Y, Hao Z, Huang C, Xia D (2019) Modification of zeolite by metal and adsorption desulfurization of organic sulfide in natural gas. J Nat Gas Eng. https://doi.org/10.1016/j.jngse.2019.102941

44. Gerards RTJ, Fernandes A, Graça I, Ribeiro MF (2020) Towards understanding of phenolic compounds impact on Ni- and V-USY zeolites during bio-oils co-processing in FCC units. Fuel. https://doi.org/10.1016/j.fuel.2019.116372

45. Paul D, Kasera N, Kolar P, Hall SG (2020) Physicochemical characterization data of pine-derived biochar and natural zeolite as precursors to catalysts. Chem Data Collect. https://doi.org/10.1016/j.cdc.2020.100573

46. Moon DJ, Lim WT (2020) Synthesis and single-crystal structure of sodium sulfide cationic cluster in the sodalite cavity of zeolite Y (FAU, Si/Al = 1.56). J Porous Mater 27(4):1233–1240. https://doi.org/10.1007/s10934-10020-00904-10931

47. Kaneko K, Ishii C, Ruike M, kuwabara H, (1992) Origin of super-high surface area and microcrystalline graphitic structures of activated carbons. Carbon 30(7):1075–1088. https://doi.org/10.1016/0008-6223(92)90139-N

48. Sing KSW (1985) Reporting physisorption data for gas/solid systems with special reference to the determination of surface area and porosity (Recommendations 1984). Pure Appl Chem 57(4):603–619. https://doi.org/10.1351/pac198557040603

49. Amari A, Chlendi M, Gannouni A, Bellagi A (2010) Optimised activation of bentonite for toluene adsorption. Appl Clay Sci 47(3):457–461. https://doi.org/10.1016/j.clay.2009.1011.1035

50. Barrett EP, Joyner LG, Halenda PP (1951) The determination of pore volume and area distributions in porous substances. I. Computations from nitrogen isotherms. J Am Chem Soc 1:373–380. https://doi.org/10.1021/ja01145a01126

51. Ozdes D, Duran C, Senturk HB (2011) Adsorptive removal of Cd(II) and Pb(II) ions from aqueous solutions by using Turkish illitic clay. J Environ Manage 92(12):3082–3090. https://doi.org/10.1016/j.jenvman.2011.3007.3022

52. Sáez P, Rodríguez A, Gómez JM, Paramio C, Fraile C, Díez E (2021) H-Clinoptilolite as an efficient and low-cost adsorbent

for batch and continuous gallium removal from aqueous solutions. J Sustain Metall 7(4):1699–1716. https://doi.org/10.1007/s40831-40021-00437-40830

53. Elwakeel KZ, El-Bindary AA, Kouta EY (2017) Retention of copper, cadmium and lead from water by Na-Y-zeolite confined in methyl methacrylate shell. J Environ Chem Eng 5(4):3698–3710. https://doi.org/10.1016/j.jece.2017.3606.3049

54. Arief VO, Trilestari K, Sunarso J, Indraswati N, Ismadji S (2008) Recent progress on biosorption of heavy metals from liquids using low cost biosorbents: characterization, biosorption parameters and mechanism studies. CLEAN – Soil. Air, Water 12:937–962. https://doi.org/10.1002/clen.200800167

55. Wang S, Vincent T, Faur C, Guibal E (2017) Modeling competitive sorption of lead and copper ions onto alginate and greenly prepared algal-based beads. Bioresour Technol 231:26–35. https://doi.org/10.1016/j.biortech.2017.1001.1066

56. Abollino O, Aceto M, Malandrino M, Sarzanini C, Mentasti E (2003) Adsorption of heavy metals on Na-montmorillonite. Effect of pH and organic substances. Water Res 7:1619–1627. https://doi.org/10.1016/S0043-1354(1602)00524-00529

57. Wang S, Dong Y, He M, Chen L, Yu X (2009) Characterization of GMZ bentonite and its application in the adsorption of Pb(II) from aqueous solutions. Appl Clay Sci 43(2):164–171. https://doi.org/10.1016/j.clay.2008.1007.1028

58. Giles CH, Smith D, Huitson A (1974) A general treatment and classification of the solute adsorption isotherm. I. Theoretical. J Colloid Interface Sci 47(3):755–765. https://doi.org/10.1016/0021-9797(1074)90252-90255

59. Neskoromnaya EA, Khamizov RK, Melezhyk AV, Memetova AE, Mkrtchan ES, Babkin AV (2022) Adsorption of lead ions (Pb^{2+}) from wastewater using effective nanocomposite GO/CMC/FeNPs: kinetic, isotherm, and desorption studies. Colloids Surf, A. https://doi.org/10.1016/j.colsurfa.2022.130224

60. Airoldi C, Critter SAM (1997) Brazilian red latosol a typic soil as an exchanger: a thermodynamic study involving Cu, Zn, Cd, Hg, Pb. Ca and Na. Clays Clay Min 45(2):125–131. https://doi.org/10.1346/CCMN.1997.0450201

61. González MT, Molina-Sabio M, Rodríguez-Reinoso F (1994) Steam activation of olive stone chars, development of porosity. Carbon 32(8):1407–1413. https://doi.org/10.1016/0008-6223(1494)90133-90133

62. Adebowale KO, Unuabonah IE, Olu-Owolabi BI (2006) The effect of some operating variables on the adsorption of lead and cadmium ions on kaolinite clay. J Hazard Mater 134(1):130–139. https://doi.org/10.1016/j.jhazmat.2005.1010.1056

63. Hang Y, Si Y, Zhou Q, Yin H, Wang A, Cao A (2019) Morphology-controlled synthesis of calcium titanate particles and adsorption kinetics, isotherms, and thermodynamics of Cd(II), Pb(II), and Cu(II) cations. J Hazard Mater. https://doi.org/10.1016/j.jhazmat.2019.120789

64. Wu D, Wang Y, Li Y, Wei Q, Hu L, Yan T, Feng R, Yan L, Du B (2019) Phosphorylated chitosan/CoFe2O4 composite for the efficient removal of Pb(II) and Cd(II) from aqueous solution: adsorption performance and mechanism studies. J Mol Liq 277:181–188. https://doi.org/10.1016/j.molliq.2018.1012.1098

65. Khaled A, El Nemr A, El-Sikaily A, Abdelwahab O (2009) Treatment of artificial textile dye effluent containing Direct Yellow 12 by orange peel carbon. Desalination 238(1):210–232. https://doi.org/10.1016/j.desal.2008.1002.1014

66. Hameed BH, Daud FBM (2008) Adsorption studies of basic dye on activated carbon derived from agricultural waste: Hevea brasiliensis seed coat. Chem Eng J 139(1):48–55. https://doi.org/10.1016/j.cej.2007.1007.1089

67. Allen SJ, McKay G, Khader KYH (1989) Intraparticle diffusion of a basic dye during adsorption onto sphagnum peat. Environ Pollut 56(1):39–50. https://doi.org/10.1016/0269-7491(1089)90120-90126

68. Qu J, Tian X, Jiang Z, Cao B, Akindolie MS, Hu Q, Feng C, Feng Y, Meng X, Zhang Y (2020) Multi-component adsorption of Pb(II), Cd(II) and Ni(II) onto microwave-functionalized cellulose: kinetics, isotherms, thermodynamics, mechanisms and application for electroplating wastewater purification. J Hazard Mater. https://doi.org/10.1016/j.jhazmat.2019.121718

69. Eren E, Cubuk O, Ciftci H, Eren B, Caglar B (2010) Adsorption of basic dye from aqueous solutions by modified sepiolite: equilibrium, kinetics and thermodynamics study. Desalination 252(1):88–96. https://doi.org/10.1016/j.desal.2009.1010.1020

70. He J, Li Y, Wang C, Zhang K, Lin D, Kong L, Liu J (2017) Rapid adsorption of Pb, Cu and Cd from aqueous solutions by β-cyclodextrin polymers. Appl Surf Sci 426:29–39. https://doi.org/10.1016/j.apsusc.2017.1007.1103

71. Sprynskyy M, Buszewski B, Terzyk AP, Namieśnik J (2006) Study of the selection mechanism of heavy metal (Pb2+, Cu2+, Ni2+, and Cd2+) adsorption on clinoptilolite. J Colloid Interface Sci 304(1):21–28. https://doi.org/10.1016/j.jcis.2006.1007.1068

72. Amarasinghe BMWPK, Williams RA (2007) Tea waste as a low cost adsorbent for the removal of Cu and Pb from wastewater. Chem Eng J 132(1):299–309. https://doi.org/10.1016/j.cej.2007.1001.1016.10.1016/j.cej.2007.01.016

73. Belviso C (2020) Zeolite for potential toxic metal uptake from contaminated soil: a brief review. Processes 8(7):820. https://doi.org/10.3390/pr8070820

74. Dai S, Wang N, Qi C, Wang X, Ma Y, Yang L, Liu X, Huang Q, Nie C, Hu B, Wang X (2019) Preparation of core-shell structure Fe3O4@C@MnO2 nanoparticles for efficient elimination of U(VI) and Eu(III) ions. Sci Total Environ 685:986–996. https://doi.org/10.1016/j.scitotenv.2019.1006.1292

75. Li S, Dong L, Wei Z, Sheng G, Du K, Hu B (2020) Adsorption and mechanistic study of the invasive plant-derived biochar functionalized with CaAl-LDH for Eu(III) in water. J Environ Sci 96:127–137. https://doi.org/10.1016/j.jes.2020.1005.1001

76. Liu L, Luo X-B, Ding L, Luo S-L (2019) 4 - Application of nanotechnology in the removal of heavy metal from water. In: Luo X, Deng F (eds) Nanomaterials for the removal of pollutants and resource reutilization. Elsevier 83-147. https://doi.org/10.1016/B1978-1010-1012-814837-814832.800004-814834

77. Hamdaoui O, Naffrechoux E (2007) Modeling of adsorption isotherms of phenol and chlorophenols onto granular activated carbon: Part I. Two-parameter models and equations allowing determination of thermodynamic parameters. J Hazard Mater 147(1):381–394. https://doi.org/10.1016/j.jhazmat.2007.1001.1021

78. Puspitasari T, Ilmi MM, Nurdini N, Mukti RR, Radiman CL, Darwis D, Kadja GTM (2019) The physicochemical characteristics of natural zeolites governing the adsorption of Pb2+ from aqueous environment. Key Eng Mater 811:92–98. https://doi.org/10.4028/www.scientific.net/KEM.4811.4092

79. Vassileva PS, Radoykova TH, Detcheva AK, Avramova IA, Aleksieva KI, Nenkova SK, Valchev IV, Mehandjiev DR (2016) Adsorption of Ag+ ions on hydrolyzed lignocellulosic materials based on willow, paulownia, wheat straw and maize stalks. Int j sci environ technol 13(5):1319–1328. https://doi.org/10.1007/s13762-13016-10970-y

80. Araújo CST, Almeida ILS, Rezende HC, Marcionilio SMLdO, León JJL, Matos TN (2018) Elucidation of mechanism involved in adsorption of Pb(II) onto lobeira fruit (Solanum lycocarpum) using Langmuir, Freundlich and Temkin isotherms. Microchem J 137:348–354. https://doi.org/10.1016/j.microc.2017.1011.1009

81. Ehrlich G (1963) Physical adsorption of gases: D.M. Young and A.D. Crowell: Butterworths, London (1962). 426 pp. 70s. J Phys Chem 24(9):1150. https://doi.org/10.1016/0022-3697(1163)90031-90033

82. Bachmann SAL, Calvete T, Féris LA (2021) Caffeine removal from aqueous media by adsorption: an overview of adsorbents

evolution and the kinetic, equilibrium and thermodynamic studies. Sci Total Environ. https://doi.org/10.1016/j.scitotenv.2020.144229

83. Gupta VK, Gupta M, Sharma S (2001) Process development for the removal of lead and chromium from aqueous solutions using red mud—an aluminium industry waste. Water Res 35(5):1125–1134. https://doi.org/10.1016/S0043-1354(1100)00389-00384

84. Hamoudi SA, Hamdi B, Brendlé J (2018) Chapter 4.7 - Removal of ions Pb2+ and Cd2+ from aqueous solution by containment geomaterials. In: Dincer I, Colpan CO, Kizilkan O (eds) Exergetic, Energetic and Environmental Dimensions. Academic Press, pp 1029–1043. https://doi.org/10.1016/B1978-1020-1012-813734-813735.800058-813735

85. Dhaouadi F, Sellaoui L, Chávez-González B, Elizabeth Reynel-Ávila H, Diaz-Muñoz LL, Mendoza-Castillo DI, Bonilla-Petriciolet A, Lima EC, Tapia-Picazo JC, Lamine AB (2021) Application of a heterogeneous physical model for the adsorption of Cd2+, Ni2+, Zn2+ and Cu2+ ions on flamboyant pods functionalized with citric acid. Chem Eng J. https://doi.org/10.1016/j.cej.2020.127975

86. Orumwense FFO (1996) Removal of lead from water by adsorption on a kaolinitic clay. J Chem Technol Biotechnol 65(4):363–369. https://doi.org/10.1002/(SICI)1097-4660(199604)199665:199604&gt199363::AID-JCTB199435&lt199603.199600.CO;199602-199603

87. Yavuz Ö, Altunkaynak Y, Güzel F (2003) Removal of copper, nickel, cobalt and manganese from aqueous solution by kaolinite. Water Res 37(4):948–952. https://doi.org/10.1016/S0043-1354(1002)00409-00408

88. Unuabonah EI, Adebowale KO, Olu-Owolabi BI, Yang LZ, Kong LX (2008) Adsorption of Pb (II) and Cd (II) from aqueous solutions onto sodium tetraborate-modified Kaolinite clay: equilibrium and thermodynamic studies. Hydrometallurgy 93(1):1–9. https://doi.org/10.1016/j.hydromet.2008.1002.1009

89. Barkat M, Nibou D, Amokrane S, Chegrouche S, Mellah A (2015) Uranium (VI) adsorption on synthesized 4A and P1 zeolites: equilibrium, kinetic, and thermodynamic studies. C R Chim 18(3):261–269. https://doi.org/10.1016/j.crci.2014.1009.1011

90. Saha UK, Taniguchi S, Sakurai K (2001) Adsorption behavior of cadmium, zinc, and lead on hydroxyaluminum– and hydroxyaluminosilicate–montmorillonite complexes. Soil Sci Soc Am J 65(3):694–703

91. Es-sahbany H, Hsissou R, El Hachimi ML, Allaoui M, Nkhili S, Elyoubi MS (2021) Investigation of the adsorption of heavy metals (Cu Co, Ni and Pb) in treatment synthetic wastewater using natural clay as a potential adsorbent (Sale-Morocco). Mater Today: Proc 45:7290–7298. https://doi.org/10.1016/j.matpr.2020.7212.1100.10.1016/j.matpr.2020.12.1100

92. Kong Q, Shi X, Ma W, Zhang F, Yu T, Zhao F, Zhao D, Wei C (2021) Strategies to improve the adsorption properties of graphene-based adsorbent towards heavy metal ions and their compound pollutants: a review. J Hazard Mater. https://doi.org/10.1016/j.jhazmat.2021.125690